Spectroscopic camera analysis of the roles of molecularly assisted reaction chains during detachment in JET L-mode plasmas

J. Karhunen [a,*], A. Holm [b], S. Aleiferis [a], P. Carvalho [a], M. Groth [b], K.D. Lawson [a], B. Lomanowski [c], A.G. Meigs [a], A. Shaw [a], V. Solokha [b], JET Contributors[1]

[a] *UKAEA, Culham Science Centre, Abingdon, OX14 3DB, UK*
[b] *Aalto University, Department of Applied Physics, Espoo, 02150, Finland*
[c] *Oak Ridge National Laboratory, Oak Ridge, TN 37831, USA*

ARTICLE INFO

ABSTRACT

The roles of the molecularly assisted ionization (MAI), recombination (MAR) and dissociation (MAD) reaction chains with respect to the purely atomic ionization and recombination processes were studied experimentally during detachment in low-confinement mode (L-mode) plasmas in JET with the help of experimentally inferred divertor plasma and neutral conditions, extracted previously from filtered camera observations of deuterium Balmer emission, and the reaction coefficients provided by the ADAS, AMJUEL and H2VIBR atomic and molecular databases. The direct contribution of MAI and MAR in the outer divertor particle balance was found to be inferior to the electron–atom ionization (EAI) and electron–ion recombination (EIR). Near the outer strike point, a strong atom source due to the D_2^+-driven MAD was, however, observed to correlate with the onset of detachment at outer strike point temperatures of $T_{e,osp} = 0.9$–2.0 eV via increased plasma-neutral interactions before the increasing dominance of EIR at $T_{e,osp} < 0.9$ eV, followed by increasing degree of detachment. The analysis was supported by predictions from EDGE2D-EIRENE simulations which were in qualitative agreement with the experimental observations.

1. Introduction

During recent years, development of different analysis methods for filtered divertor camera observations of the deuterium Balmer emission lines at, e.g., ASDEX Upgrade [1], MAST Upgrade [2], JET [3,4] and TCV [5] has made significant progress in provision of experimentally inferred localized 2D estimates for the electron temperature, T_e, electron density, n_e, and the atomic density, n_{at}, in the divertor volume. Application of novel methods [6–10] for distinguishing the Balmer emission components arising from molecular processes [6,11, 12] — which have been observed to even strongly dominate the total Balmer D_α intensity at the onset of detachment [6–9,12–16] — has further enabled inference of the molecular divertor density, n_{mol}, as well as the contributions of different molecular reactions in ionization and recombination. Together, these methods facilitate comprehensive emission-based 2D analysis of the divertor plasma conditions and the roles of atomic and molecular processes in divertor detachment and particle balance.

In this work, the roles of atomic and molecular reactions and reaction chains have been studied during detachment of the outer divertor in low-confinement mode (L-mode) plasmas in JET. The analysis relies on divertor plasma conditions inferred experimentally earlier in [3,4, 8,9] from intensity ratios of reflection-corrected tomographic reconstructions [17] of the Balmer D_α, D_γ and D_ϵ emission lines, observed with the tangential filtered divertor camera system of JET [18]. The experimental observations are compared qualitatively to predictions of EDGE2D-EIRENE [19–21] simulations.

2. Atomic and molecular reaction chains

During the course of detachment, the divertor plasma is characterized by a range of atomic and molecular reactions and reaction chains with widely reported varying effects on the particle balance and the detachment process [6,7,22–29]. The atomic and molecular processes considered in this work are compiled in Table 1 and — depending on their potential net effect on the change in the number of D^+ ions,

---

Table 1
Purely atomic electron–atom ionization (EAI) and electron–ion recombination (EIR) reactions and the molecularly assisted dissociation (MAD), ionization (MAI) and recombination (MAR) reactions and reaction chains considered in the analysis, together with their net effect on the number of D_2 molecules (ΔD_2), D atoms (ΔD) and D^+ ions (ΔD^+).

1st reaction	2nd reaction	ΔD_2	ΔD	ΔD^+	Type
$e + D \rightarrow 2e + D^+$	–		± 0	-1	$+1$	EAI
$e + D^+ \rightarrow D$	–		± 0	$+1$	-1	EIR
$e + D_2 \rightarrow e + 2D$	–	-1	$+2$	± 0	MAD
$e + D_2 \rightarrow 2e + D + D^+$	–	-1	$+1$	$+1$	MAD, MAI
$D^+ + D_2 \rightarrow D_2^+ + D$	$e + D_2^+ \rightarrow 2D$	-1	$+3$	-1	MAD, MAR
	$e + D_2^+ \rightarrow e + D + D^+$	-1	$+2$	± 0	MAD
	$e + D_2^+ \rightarrow 2e + 2D^+$	-1	$+1$	$+1$	MAD, MAI
$e + D_2 \rightarrow 2e + D_2^+$	$e + D_2^+ \rightarrow 2D$	-1	$+2$	± 0	MAD
	$e + D_2^+ \rightarrow e + D + D^+$	-1	$+1$	$+1$	MAD, MAI
	$e + D_2^+ \rightarrow 2e + 2D^+$	-1	± 0	$+2$	MAD, MAI

ΔD^+, in the divertor plasma — further classified to ionizing ($\Delta D^+ > 0$) and recombining ($\Delta D^+ < 0$) processes. The purely atomic processes consist of electron–atom ionization (EAI, $\Delta D^+ = +1$) and electron–ion recombination (EIR, $\Delta D^+ = -1$) which occur between electrons, D atoms and D^+ ions without contributions from D_2 molecules.

All of the molecular processes in Table 1 lead to dissociation of a D_2 molecule and are thus categorized as molecularly assisted dissociation (MAD, $\Delta D_2 < 0$). For simplified distinction between purely atomic and molecular processes in the context of this work, direct electron-impact dissociation of D_2 into D atoms and D^+ ions is treated as MAD together with the established MAD processes taking place as two-step reaction chains via formation and reactions of molecular D_2^+ ions. As noted in Table 1, some of these reactions and reaction chains increase or decrease the number of D^+ ions in the plasma and can thus be classified as molecularly assisted ionization (MAI, $\Delta D^+ > 0$) and recombination (MAR, $\Delta D^+ < 0$), respectively. Molecular processes involving negative D^- ions and molecular D_3^+ ions have been omitted due to the insignificant presence of these species in deuterium plasmas at divertor-relevant conditions [30–33].

While only one D_2^+-driven MAD chain can be directly categorized as MAR, Table 1 suggests that all MAD chains apart from one lead to an increased number of atoms ($\Delta D > 0$). This poses the MAD chains as potential favourable precursors for detachment due to their enhancing effect on momentum and power losses in the divertor via plasma–atom interactions. The MAD processes are thus discussed in this work in light of their roles as sources for atoms.

For the analysis discussed here, the reaction rates for the processes compiled in Table 1 have been calculated with the help of the ADAS database [34] in the case EIR and the AMJUEL [35] and H2VIBR [36] atomic and molecular databases of EIRENE for the MAD, MAI and MAR reactions, using the experimentally inferred estimates for T_e, n_e, n_{at} and n_{mol} presented in [3,4,8,9]. Due to the limited ability of the experimental analysis method to track the outer divertor ionization front during detachment, as discussed in [4], global EAI was not calculated directly with ADAS coefficients but estimated based on the outer divertor particle balance as

$$R_{EAI} = \Phi_{ot} + R_{EIR} + R_{MAR} - R_{MAI}, \tag{1}$$

where Φ_{ot} is the ion current integrated over the outer target, and $R_{EAI/EIR/MAR/MAI} = \int S_{EAI/EIR/MAR/MAI} dV_{div}$ are integrals of the local EAI, EIR, MAR and MAI rates, $S_{EAI/EIR/MAR/MAI}$, over the outer divertor volume, V_{div}. The validity of this estimate is discussed in Section 4. The effect of the vibrational excitation of the D_2 molecules in calculations of the molecular reaction rates has been accounted for with the Python tool CRUMPET [37], as described in [9].

3. Roles of atomic and molecular reaction chains during L-mode detachment

The roles of the atomic and molecular reactions and reaction chains were studied experimentally during an L-mode density scan in JET, consisting of pulses 94 759, 94 771 and 94 773, supported by an EDGE2D-EIRENE density scan covering an approximately similar input parameter range. The experiment and the simulations are described in more detail in [4,38]. During the scans, the outer divertor ranged from high-recycling to deeply detached conditions, as visualized by the decrease of the outer target ion current in Fig. 1a and e, as the outer strike point electron temperature, $T_{e,osp}$, decreases down to $T_{e,osp} \approx 0.5$ eV. As suggested by Fig. 1e, the EDGE2D-EIRENE scan failed to predict as deep detachment in terms of decreasing Φ_{ot} as observed experimentally despite reaching equally low divertor temperatures, which was attributed in [4,9] to the 3–4 times lower divertor n_e and the resulting shortfall of EIR in the simulations due its approximate n_e^2 dependence. No attempts for accurate quantitative match between the simulations and the experiment were made, and the comparisons made in this work are predominantly qualitative.

3.1. $T_{e,osp} > 2.0$ eV: ionizing outer strike point region

In high-recycling conditions with $T_{e,osp} > 2.0$ eV, Fig. 1b and f show prominent EAI and MAI components at the outer strike point decreasing with decreasing $T_{e,osp}$, together with a strong atom source due to molecular dissociation peaking at $T_{e,osp} = 3$–4 eV. The break-up of the atom source into the different reaction contributions in Fig. 2a and c suggests it being dominated by the direct single-step electron-impact dissociation of the D_2 molecules into two D atoms with a smaller contribution from the $e + D_2^+ \rightarrow e + D + D^+$ MAD chain, for which the D_2^+ ions are generated in collisions of electrons and D_2 molecules. The latter chain is also responsible for the observed MAI contribution.

The atomic and molecular densities at the outer strike point in Fig. 1d and h remain low in this temperature range with EAI dominating the global investigation in Fig. 1c and g. The outer divertor can thus be characterized as ionizing with a significant MAI contribution in the outer strike point region. The EDGE2D-EIRENE predictions show more emphasis on EAI at the outers strike point, increasing steadily with $T_{e,osp}$ by a factor of 2–3 beyond the limit of the y scale in Fig. 1f. At $T_{e,osp} < 2.5$ eV, the ionization is virtually absent at the outer strike point in the simulations, which even leads to appearance of unphysical negative values in Fig. 1f due to numerical fluctuations.

3.2. $T_{e,osp} = 0.9$–2.0 eV: dominant atom source due to D_2^+-driven MAD

The decrease of $T_{e,osp}$ to $T_{e,osp} < 2.0$ eV is met with suppression of EAI, resurging increase of MAI and the MAD atom source, as well as emergence of EIR and MAR at the outer strike point in Fig. 1b and f. Unlike in the high-recycling conditions, the increase in MAD is almost entirely driven by the $e + D_2^+ \rightarrow e + D + D^+$ chain with the D_2^+ generated in collisions of D^+ ions and D_2 molecules, as seen in Fig. 2a and c. MAI, instead, is dominated by the same D_2^+-driven reaction chain as in the high-recycling conditions. This D_2^+-driven MAD chain is responsible also for the global MAD surge, as shown in Fig. 2b and d, making the global atom source exceed the global ionization rate at $T_{e,osp} \lesssim 1.5$ eV in Fig. 1c and g.

Closer inspection of the ionization–recombination balance at the outer strike point in Fig. 3 indicates that the increasing EIR, MAR and MAI contributions approximately cancel each other at $T_{e,osp} = 0.9$–2.0 eV in the experimental analysis, leaving the outer strike point region effectively neither ionizing nor recombining. In the absence of a net recombination source, the steep increase in the atomic density with decreasing $T_{e,osp}$ in Fig. 1d can thus be attributed to the atoms resulting from MAD avoiding the prompt ionization characteristic to higher divertor temperatures. It is, however, noted that the peak n_{at} value
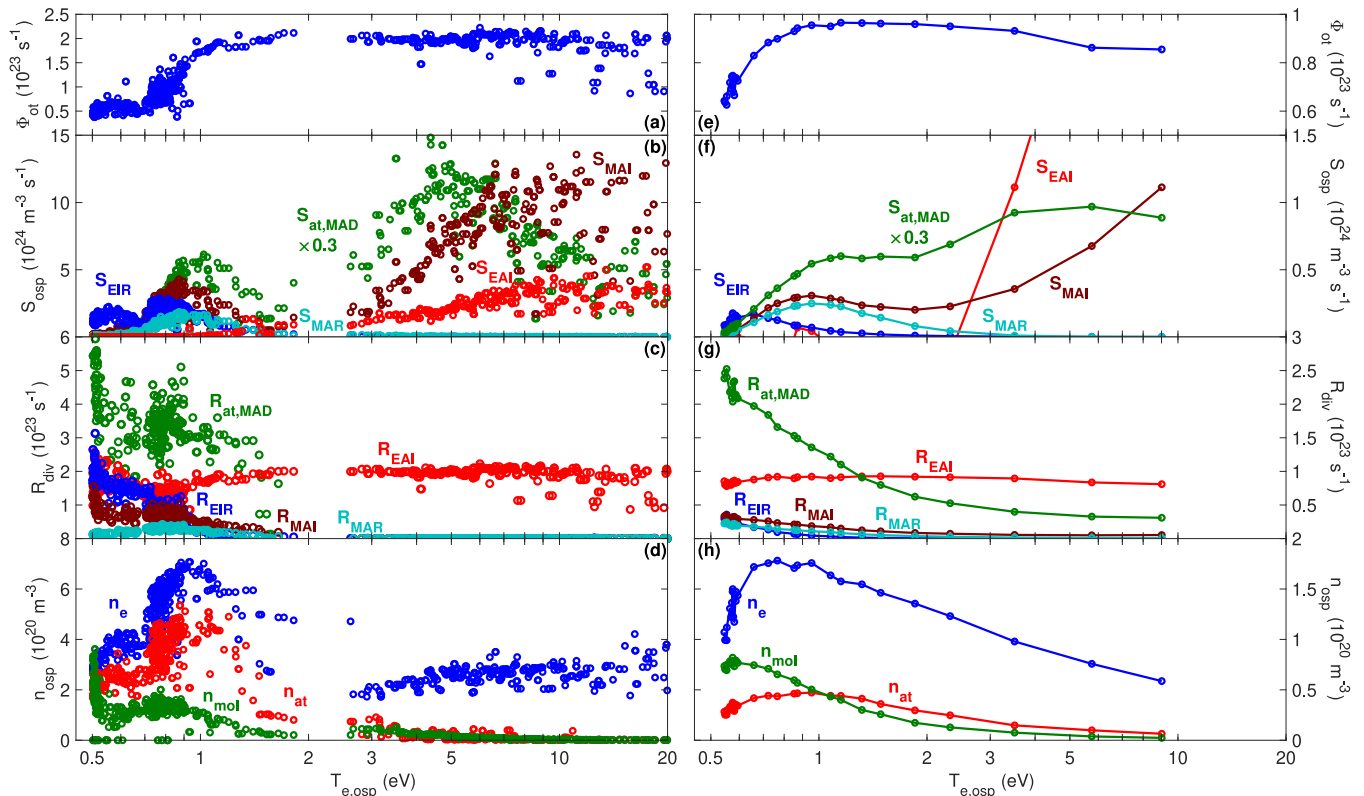
Fig. 1. Integrated outer target ion currents (a, e) and reaction rates of EAI (red), EIR (blue), MAI (dark red), MAR (cyan) and the MAD atom source (green) locally at the outer strike point (b, f) and integrated across the outer divertor volume (c, g) together with electron (blue), atomic (red) and molecular (green) densities at the outer strike point (d, h) as functions of the outer strike point electron temperature for the experimental analysis (a–d) and the EDGE2D-EIRENE simulations (e–h). The y axes in (e, f) have been truncated and the data for the MAD atom source multiplied by a factor of 0.3 in (b, f) for illustrative purposes. Note the logarithmic x axes. (For interpretation of the references to colour in this figure legend, the reader is referred to the web version of this article.)
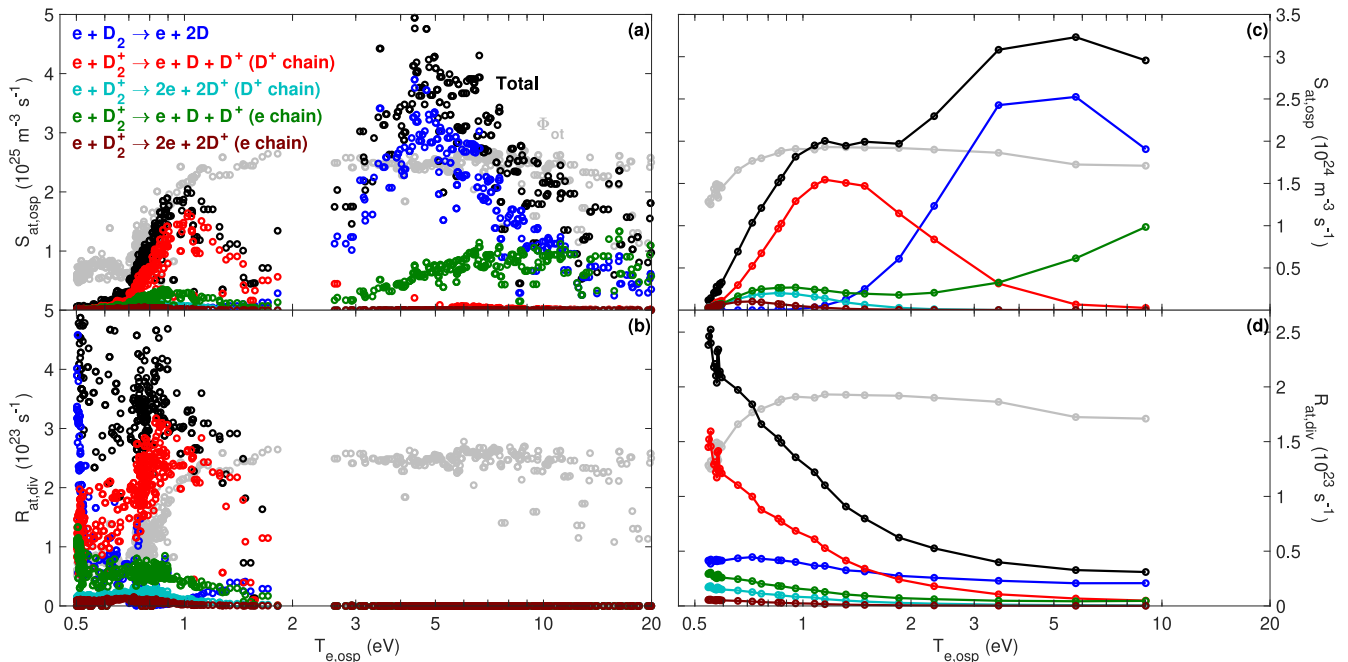

Fig. 2. Breakdown of the MAD atom source into contributions from different reaction chains at the outer strike point (a, c) and integrated across the outer divertor volume (b, d) as a function of the outer strike point electron temperature for the experimental analysis (a, b) and the EDGE2D-EIRENE simulations (c, d). The colour coding of the different reaction chains applies in all subplots according to the legend in (a), while the black data denotes the total rate as a sum of the components, and the grey data represents the target ion current as a guideline for the detachment process. The reactions chains presented in Table 1 but not included in this figure were found to yield insignificant contributions to the total atom source. Note the logarithmic x axes. (For interpretation of the references to colour in this figure legend, the reader is referred to the web version of this article.)
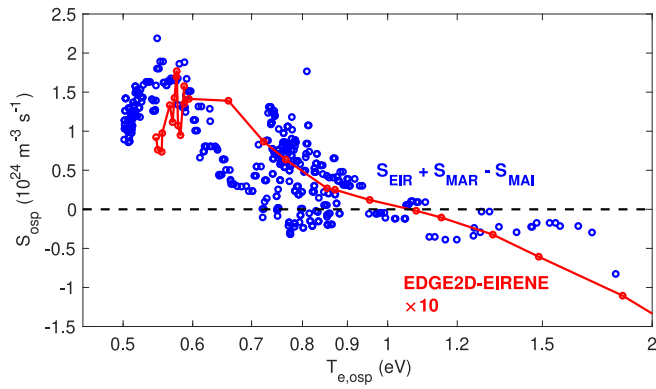
Fig. 3. The ionization–recombination balance at the outer strike point calculated form the experimentally inferred reaction rates (blue) and the EDGE2D-EIRENE predictions (red) as a function of the outer strike point electron temperature across the range of $T_{e,osp} = 0.5$–2.0 eV. Positive values indicate dominance of EIR and MAR over MAI and vice versa. The ionization–recombination balance calculated from the EDGE2D-EIRENE predictions has been scaled by a factor of 10 for illustrative purposes. Note the logarithmic x axis. (For interpretation of the references to colour in this figure legend, the reader is referred to the web version of this article.)

is prone to overestimation, as discussed in [9]. The increasing atomic density provides favourable conditions for momentum and power losses via plasma–atom interactions, consequently promoting the onset of detachment of the outer divertor, as supported by Φ_{ot} in Fig. 1a turning to decrease across this temperature range. In the EDGE2D-EIRENE simulations, the decrease of Φ_{ot} begins closer to $T_{e,osp} \approx 1.0$ eV in Fig. 1e, which is likely due to MAI dominating the ionization–recombination balance in Fig. 3 at $T_{e,osp} \gtrsim 1.2$ eV.

3.3. $T_{e,osp} < 0.9$ eV: recombining outer strike point region

As the divertor temperature decreases to below $T_{e,osp} = 1.0$ eV, EIR gains significance in Fig. 1b and f, while both MAR and MAI turn to decrease. As a consequence, the ionization–recombination balance in Fig. 3 suggests the outer strike point region becoming dominated by recombination processes at $T_{e,osp} \lesssim 0.9$ eV. In both the experimental analysis and the EDGE2D-EIRENE predictions, the transition to recombining conditions in the outer strike point region coincides with significantly steepening decrease of Φ_{ot} in Fig. 1a and e, highlighting the integral role of EIR in the detachment process. The experimental analysis indicates EIR dominating over MAI and MAR across the outer divertor volume at $T_{e,osp} < 0.9$ eV in Fig. 1c, whereas EDGE2D-EIRENE predicts its contribution to be lower than that of MAI and of the same order as for MAR in Fig. 1g. This is attributed to the previously mentioned difference in the divertor density and is likely the reason for Fig. 1e not showing as high degree of detachment as observed experimentally in Fig. 1a.

4. Spatial restrictions of the experimental observation of MAI and MAR contributions in total ionization and recombination

As discussed in [4], the spatial coverage of the analysis method behind the inference of the T_e, n_e, n_{at} and n_{mol} estimates is restricted by its reliance on the recombination-dominated D_ε emission. This can affect the global investigation of the ionization and recombination processes and the conclusions drawn on the outer divertor particle balance based on the emission data. The potential effects of the spatially restricted observations on the global analysis have been studied in Fig. 4a by comparing the volume integrals of the different reaction rates across the entire outer divertor volume and the volume in which the D_ε emission intensity exceeds 15% of its peak value, which is the criterion stated in [4] for the experimental analysis method to guarantee an adequate signal-to-noise ratio.

As already noted in [4], Fig. 4a indicates the emission-based analysis being capable of observing up to 80% of the EIR events in detached conditions, whereas the global EAI is heavily underestimated when calculated directly from the plasma parameters due to the lack of overlap between the recombination-driven D_ε emission region and the upstream-shifting ionization front. Instead, when calculated with the help of the outer divertor particle balance according to Eq. (1), the resulting R_{EAI} agrees within 2% of the true global EAI rate and deviates from it only by approximately 5%, when only the EIR, MAI and MAR occurring within the D_ε emission region are taken into account in Eq. (1).

When the observations are restricted to the D_ε emission region, the EDGE2D-EIRENE simulations in Fig. 4a predict that approximately 50% of the MAI and MAR events remain unaccounted for. This is due to the spatial distribution of the D_2 molecules spreading radially further into the divertor SOL than the D_ε emission which tends to remain closer to the separatrix. Consequently, while the regions with the strongest MAI and MAR activity are captured by the experimental method, the weaker regions are beyond its spatial coverage.

The incomplete observation of the MAI and MAR reactions can lead to underestimation of their roles in the global outer divertor particle balance, as visualized in Fig. 4b, presenting the fractions of MAI and MAR in the total ionization and recombination events, respectively. The experimental analysis suggests MAI to be responsible for less than 20% of the ionization events at $T_{e,osp} > 1.0$ eV, while its fraction increases to 30%–50% in deepening detachment, when the molecular divertor density is observed to increase in Fig. 1d. The corresponding EDGE2D-EIRENE analysis in the same figure, however, indicates that the experimentally inferred MAI fraction could be up to a factor of 2 too low with respect to the true MAI fraction across the outer divertor volume.

In the case of recombination, the experimental analysis shows peak MAR fractions of up to 60% at $T_{e,osp} \approx 1.0$–1.5 eV, coinciding with the emergence of both MAR and EIR in Fig. 1c and the strongest dominance of the D_2^+-driven molecularly induced emission component in the total D_α intensity observed in [8,9]. Below $T_{e,osp} \approx 1.0$ eV, the role of MAR decreases steeply with decreasing $T_{e,osp}$ to below 10% in deep detachment, when EIR dominates recombination in the outer divertor volume. As for MAI, the EDGE2D-EIRENE analysis indicates underestimation of the total MAR fraction due to the spatial restrictions of the method — but unlike for MAI, the restricted observation agrees within 20% with the true fraction, apart from the $T_{e,osp} > 2.0$ eV region, where the restricted view yields a similar decreasing trend for the MAR fraction as observed in the experimentally inferred data. Instead, the predicted true MAR fraction across the entire outer divertor volume keeps slightly increasing with $T_{e,osp}$, which is attributed to the absence of EIR at high T_e and low n_e in the OSP region and the prolonged presence of recycled D_2 in remote areas of the divertor, where T_e remains low even at elevated $T_{e,osp}$. It is noted, though, that the absolute global MAR and EIR rates are low at these temperatures, as shown in Figs. 1c and g and 4a.

The fraction of MAR of the recombination predicted by the EDGE2D-EIRENE is consistently higher than the experimentally inferred fraction, remaining above 40% even at $T_{e,osp} < 1.0$ eV. This is attributed to the previously discussed underprediction of the simulated divertor density, which affects EIR more drastically than MAR, MAI and EAI due to the approximate n_e^2 dependence of EIR. If the shortfall of the divertor n_e is crudely compensated by multiplying it by a factor of 3 in the calculation of the EIR and MAR rates from the EDGE2D-EIRENE output, the discrepancy to the experimentally inferred MAR fraction is observed to narrow significantly. This supports earlier observations — discussed in, e.g., [7,24,26–28] — of MAR having a noticeable role in divertor recombination mainly at low densities, when EIR is largely absent, while EIR becomes dominant at the high divertor densities observed experimentally during L-mode detachment in JET.
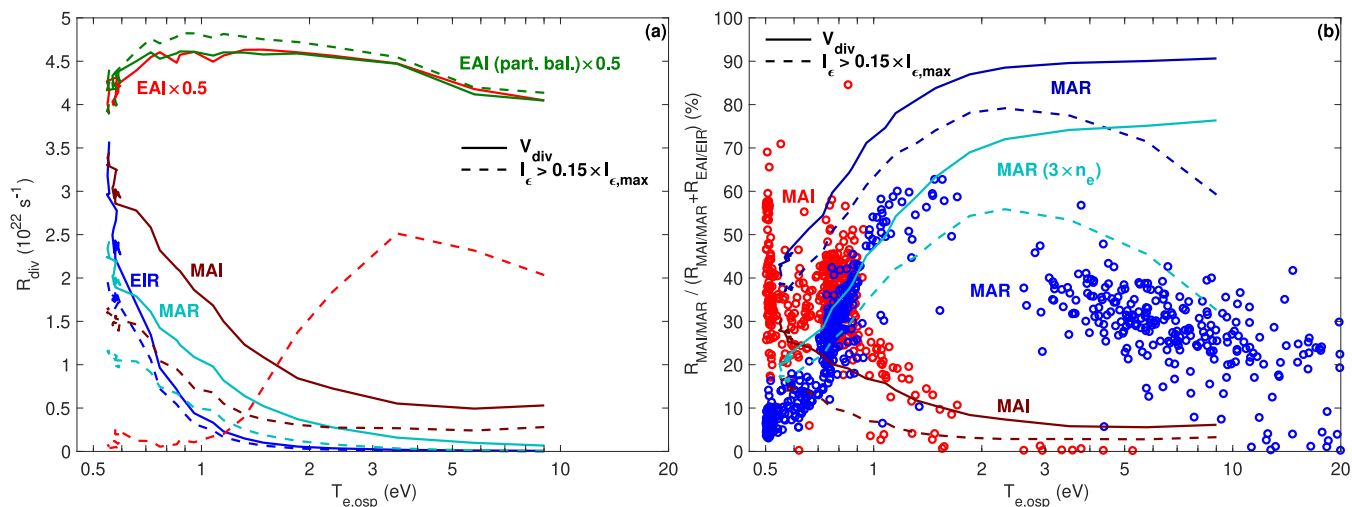
Fig. 4. Global reaction rates of EAI (red), EAI calculated from the particle balance (green), EIR (blue), MAI (dark red) and MAR (cyan) as functions of the outer strike point electron temperature (a). Experimentally inferred (data points) and EDGE2D-EIRENE predictions (curves) of the relative fractions of MAI (red) and MAR (blue) of the total ionization and recombination events with an additional EDGE2D-EIRENE prediction with the divertor n_e scaled by a factor of 3 in the calculation (cyan) as functions of the outer strike point electron temperature (b). In both subplots, the solid curves correspond to volume integrals across the entire outer divertor volume, whereas the dashed curves represent integrals across the D_ε emission region. The EAI rates in (a) have been scaled by a factor of 0.5 for illustrative purposes. Note the logarithmic x axes. (For interpretation of the references to colour in this figure legend, the reader is referred to the web version of this article.)

5. Conclusions

The roles of atomic and molecular processes in L-mode detachment were studied experimentally at JET by calculating purely atomic and molecularly assisted ionization and recombination rates based on local estimates of the divertor T_e, n_e, n_{at} and n_{mol} inferred previously from filtered camera observations of deuterium Balmer emission. Qualitative references for the experimental analysis were provided by corresponding post-processing of an EDGE2D-EIRENE density scan with an approximately similar input parameter range as in the experiment.

The direct role of molecularly assisted ionization and recombination to the outer divertor particle balance was found to be inferior to the corresponding purely atomic reactions. The contribution of D_2^+-driven MAI in outer divertor ionization was observed to increase in detached conditions with outer strike point temperatures below 1.0 eV, while remaining below 40% of the total ionization events. The fraction of the MAR reactions in the total recombination events was found to peak at approximately 60% — but only at the onset of recombination processes at $T_{e,osp} = 1.0$–2.0 eV, whereas the increasing prevalence of recombination in detached conditions at $T_{e,osp} < 1.0$ eV was predominantly attributed to the purely atomic EIR reactions, accounting for up to 90% of the recombination events in deep detachment. It is, however, noted that the inferred MAI and MAR fractions may be underestimated due to spatial restrictions of the applied experimental methodology, as suggested by the EDGE2D-EIRENE analysis.

Despite the lesser direct role of MAI and MAR, the molecularly assisted dissociation chains involving D_2^+ were found to act as significant sources of atoms at the onset of detachment. At outer strike point temperatures of $T_{e,osp} = 0.9$–2.0 eV, when the ionization and recombination processes were in balance in the outer strike point region, the observed steep increase of atomic density at the strike point in absence of a net recombination source was attributed to the D_2^+-driven MAD atom source and the absence of a net ionization sink. This was postulated to provide a favourable precursor for detachment via increased plasma-neutral interactions, supported by the roll-over and onsetting decrease of the outer target ion current within the same temperature range. At $T_{e,osp} < 0.9$ eV, the experimentally inferred recombination rates were observed to overcome MAI near the outer strike point — mainly due to increasing EIR — making the strike point region recombining, which was found to coincide by significantly steepening decrease of the target ion current towards deep detachment with further decrease of $T_{e,osp}$.

The experimentally inferred evolution of the different atomic and molecular phenomena — with its good correlation with the independent Langmuir probe measurements of the outer target ion current — is in accordance with the established description of the detachment process [39, and therein], suggesting an integral role of the molecular processes in facilitating the onset of detachment and dominance of purely atomic recombination in further development to deepening detachment. The importance of EIR is supported by the EDGE2D-EIRENE simulations which, despite primarily showing good qualitative agreement with the experimental observations, fail to reach as deep detachment, having predicted significantly lower EIR rates in the divertor than inferred experimentally, which is fundamentally attributed to underestimation of the simulated divertor n_e by a factor of 3–4.

CRediT authorship contribution statement

J. Karhunen: Conceptualization, Methodology, Software, Formal analysis, Investigation, Writing – original draft, Visualization. **A. Holm:** Conceptualization, Formal analysis. **S. Aleiferis:** Investigation. **P. Carvalho:** Investigation. **M. Groth:** Investigation, Supervision. **K.D. Lawson:** Investigation. **B. Lomanowski:** Conceptualization, Formal analysis. **A.G. Meigs:** Investigation. **A. Shaw:** Investigation. **V. Solokha:** Methodology, Software.

Declaration of competing interest

The authors declare that they have no known competing financial interests or personal relationships that could have appeared to influence the work reported in this paper.

Data availability

Data will be made available on request.

Acknowledgements

References

[1] M. Agostini, et al., Plasma Phys. Control. Fusion 61 (2019) 115001.
[2] C. Bowman, et al., Plasma Phys. Control. Fusion 62 (2020) 045014.
[3] J. Karhunen, et al., Nucl. Mater. Energy 25 (2020) 100831.
[4] J. Karhunen, et al., Plasma Phys. Control. Fusion 63 (2021) 085018.
[5] A. Perek, et al., Nucl. Fusion 62 (2022) 096012.
[6] K. Verhaegh, et al., Plasma Phys. Control. Fusion 63 (2021) 035018.
[7] K. Verhaegh, et al., Nucl. Mater. Energy 26 (2021) 100922.
[8] J. Karhunen, et al., J. Instrum. 17 (2022) C01032.
[9] J. Karhunen, et al., Plasma Phys. Control. Fusion 64 (2022) 075001.
[10] K. Verhaegh, et al., Nucl. Fusion (2022) in press.
[11] D. Wünderlich, et al., Atoms 4 (2016) 26.
[12] D. Reiter, et al., 23rd International Conference on Plasma Surface Interactions in Controlled Fusion Devices, 2018.
[13] S. Menmuir, et al., J. Quant. Spectrosc. Radiat. Transfer 105 (2007) 425–437.
[14] B. Lomanowski, et al., 23rd International Conference on Plasma Surface Interactions in Controlled Fusion Devices, 2018.
[15] M. Groth, et al., Nucl. Mater. Energy 19 (2019) 211–217.
[16] R. Dey, et al., Nucl. Fusion 59 (2019) 076005.
[17] J. Karhunen, et al., Rev. Sci. Instrum. 90 (2019) 103504.
[18] A. Huber, et al., Rev. Sci. Instrum. 83 (2012) 10D511.
[19] R. Simonini, et al., Contrib. Plasma Phys. 34 (1997) 368.
[20] D. Reiter, et al., J. Nucl. Mater. 196–198 (1992) 80–89.
[21] S. Wiesen, EDGE2D/EIRENE Code Interface Report, JET ITC-Report, 2006, www.eirene.de/e2deir_report_40jun06.pdf.
[22] R.K. Janev, et al., J. Nucl. Mater. 121 (1984) 10–16.
[23] S.I. Krasheninnikov, et al., Phys. Lett. A 214 (1996) 285–291.
[24] U. Fantz, et al., J. Nucl. Mater. 290–293 (2001) 367–373.
[25] A.Y. Pigarov, Phys. Scr. T96 (2002) 16–31.
[26] E.M. Hollmann, et al., Plasma Phys. Control. Fusion 48 (2006) 1165–1180.
[27] A.S. Kukushkin, et al., Nucl. Mater. Energy 12 (2017) 984–988.
[28] M. Sakamoto, et al., Nucl. Mater. Energy 12 (2017) 1004–1009.
[29] A. Terakado, et al., Nucl. Mater. Energy 20 (2019) 100679.
[30] J.N. Bardsley, J.M. Wadehra, Phys. Rev. A 20 (1979) 1398–1405.
[31] E. Krishnakumar, et al., Phys. Rev. Lett. 106 (2011) 243201.
[32] D. Rapp, et al., Phys. Rev. Lett. 14 (1965) 533.
[33] R.K. Janev, et al., Collision processes in low-temperature hydrogen plasmas, 2003, Jül-4105.
[34] H.P. Summers, The ADAS User Manual, Version 2.6, 2004, http://www.adas.ac.uk.
[35] D. Reiter, The data file AMJUEL: Additional Atomic and Molecular Data for EIRENE, 2020, http://www.eirene.de/amjuel.pdf.
[36] D. Reiter, The data file H2VIBR: Additional Atomic and Molecular Data for EIRENE, 2017, http://www.eirene.de/h2vibr.pdf.
[37] A. Holm, et al., Nucl. Mater. Energy 27 (2021) 100982.
[38] M. Groth, et al., Nucl. Fusion 53 (2013) 093016.
[39] S.I. Krasheninnikov, et al., J. Plasma Phys. 83 (2017) 155830501.